MAE 155B Team 9 (LiFT) CDR Report

Kyle Avery*, Andrew Fletcher†, Michael Gelnak‡, Christopher Jun§, Wilson Li¶, and Carlos Quintero‖
University of California San Diego, La Jolla, California, 92023

New, efficient, and environmentally friendly forms of transformation are needed to avoid the growing urban traffic congestion. To fix this issues, project LiFT was created to design an eVTOL aircraft with the goal to quickly and safely transport a payload while also utilizing existing infrastructure. With the goal of optimizing the range of the aircraft, an eVTOL aircraft was designed with 10 vertical propellers and 1 cruise propeller that will be able to transport a maximum of 4 passengers or 500 kgs at a cruise velocity of 50 m/s. This will allow for an allowable range of 548 kms, allowing for a round trip from San Diego to the Arizona border or a one way trip to Las Vegas.

*Undergraduate Student, Department of Mechanical and Aerospace Engineering
†Undergraduate Student, Department of Mechanical and Aerospace Engineering
‡Undergraduate Student, Department of Mechanical and Aerospace Engineering
§Undergraduate Student, Department of Mechanical and Aerospace Engineering
¶Undergraduate Student, Department of Mechanical and Aerospace Engineering
‖Undergraduate Student, Department of Mechanical and Aerospace Engineering

I. Introduction

In this day and age, humans mainly rely on automobiles for short range transportation. As the population in urban areas increases faster than the transportation infrastructure, the consequences of traffic congestion continue to rise [1]. The creation of additional infrastructure for ground-based transportation requires significant space, funding, and time [2]. An alternative is to add an additional form of transportation: short range eVTOL aircraft (electric vertical take-off and landing). By taking to the skies, traffic congestion is alleviated by moving vehicles off of the existing infrastructure to the air, where additional physical infrastructure is not necessary. From an environmental standpoint, these electric aircraft can decrease the number of gasoline vehicles as well as their corresponding harmful emissions caused by idling in traffic. eVTOL aircraft could be used as personal vehicles or applied to rideshare applications by companies such as Uber, Lyft, or taxi companies. Additionally, this application could also be marketed to the military for base to base transportation as well as shipping companies like UPS, Fedex, or Amazon as a method of delivering packages from warehouses. While there are existing designs for eVTOL aircraft, these designs are still in the concept or prototype phase, and phase limitations in range, safety, and utility.

II. Mission

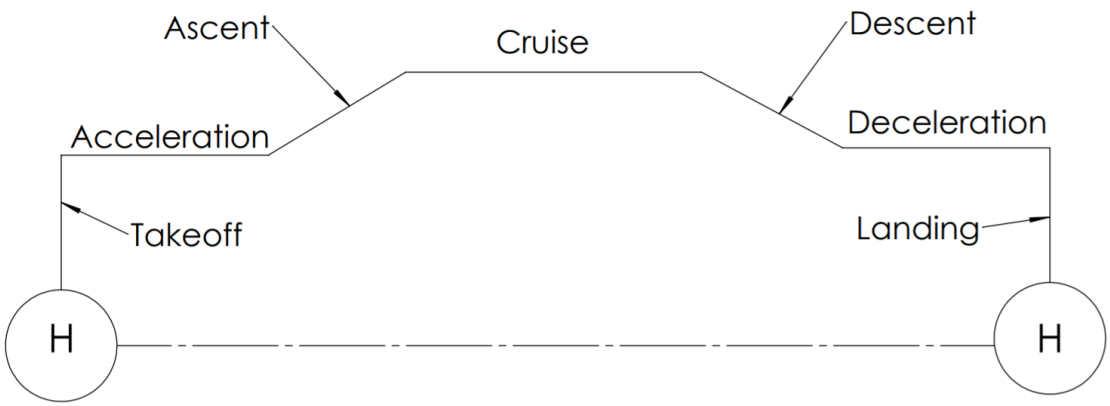

Fig. 1 LiFT eVTOL Mission Profile

The mission that the LiFT aircraft design will be based upon is a medium range flight from a helipad in San Diego to another location in Southern California such as Los Angeles or Santa Barbara. This typical mission is used as an example because it would solve many of the traffic congestion problems on Interstate 5 between San Diego and Los Angeles as well as being in tune with our team's design goal of maximum range. Figure 1 shows the typical mission profile and Table 1 shows the various mission segments for this example. First, the eVTOL aircraft will take off vertically using only the VTOL motors to 30 m at 6 m/s from an existing helipad in the San Diego area. From there, it will accelerate from 0 m/s horizontally to 35 m/s, or to just over the stall speed. During this phase, all motors will be active, but the VTOL motors will only be used for hovering until the aircraft has accelerated enough to ascend with just the cruise propeller. This acceleration phase is analogous to the takeoff of a conventional aircraft. After that, the aircraft will start the ascent phase, where the VTOL motors will disengage and the aircraft will begin to gain altitude at a climb gradient of 7 degrees to a cruising altitude of 1500 m. After reaching cruising altitude, the aircraft will transition to level flight at a speed of 50 m/s to near the landing location before descending. Much like the climb phase, the descent phase will have a descent gradient of 7 degrees until about 30 m above the landing location. From here, the VTOL motors will reengage to keep the aircraft at altitude while the aircraft begins a deceleration phase from 35 m/s to 0 m/s. The aircraft will then descend to a suitable helipad at the landing spot vertically using only the VTOL rotors at 6 m/s.

The main motivation for adding two stages for acceleration and deceleration are to reduce the time spent in the VTOL stage. Doing this significantly increases the range because the VTOL stage is five times less efficient than the cruise stage (estimate based on flight time). After clearing any surrounding buildings or trees in the vertical takeoff stage, the VTOL motors are kept on just enough to keep the aircraft in the air while building horizontal speed before a conventional ascent.

Table 1 Typical Mission

Mission segment	Speed	Altitude	Distance	Time	VTOL motors	Cruise motor
Vertical Takeoff	6 m/s	0 m -> 30 m	30 m	7 s	X	
Acceleration	0 m/s -> 35 m/s	30 m	400 m	23 s	X	X
Ascent at 7 deg	35 m/s -> 50 m/s	30 m -> 1500 m	12 km	4 min		X
Cruise	50 m/s	1500 m	250 km	80 min		X
Descent at 7 deg	50 m/s -> 35 m/s	1500 m -> 30 m	12 km	4 min		X
Deceleration	35 m/s -> 0 m/s	30 m	400 m	23 s	X	X
Vertical Landing	6 m/s	30 m -> 0 m	30 m	7 s	X	

III. Configuration

In the current world of eVTOL aircraft, five main design concepts exist. These are: multicopter, lift + cruise, tilt-rotor, tilt-wing, and ducted vector thrust. Each of these aircraft configurations have their own strengths and weaknesses. To accurately analyze the available options, a few key objectives were the focus for choosing a concept. These objectives were proven ability, propulsive efficiency, maneuverability, reliability, weight, and drag. These six design criteria were given weights from one to five based on their importance to the mission, and the multi-weighted screening model for deciding the initial concept can be seen in the table below.

Table 2 VTOL Aircraft Configurations and Design Criteria With Weights

Configuration	Proven Ability	Propulsive Efficiency	Maneuverability	Reliability	Weight	Drag	Total
Parameter Weight	4	4	1	5	3	3	
Multicopter	1	1	5	5	1	1	44
Lift + Cruise	**5**	**5**	**2**	**4**	**2**	**2**	**74**
Tilt-Rotor	4	3	4	2	4	5	69
Tilt-Wing	2	2	3	1	5	4	51
Vectored Thrust	3	4	1	3	3	3	62

Looking at the scores from the weighted screening model, the Lift + Cruise configuration had the highest weighted score. This is mainly due to the high weights that were given to reliability and proven ability metrics. UAM eVTOL have been researched for years and there are many proven Lift + Cruise working prototypes. These aircraft are also very reliable due to their use of a large number of rotors. Should one rotor fail, there are many others to provide a safe landing. This is especially important for a populous urban environment where safety is the highest priority.

Moving on, a more detailed Lift + Cruise configuration needs to be selected. Aspects of the model such as number of lifting surfaces, wing location, cruise rotor location, lift rotor location, and number of rotors needs to be decided. For lifting surfaces, four configurations were considered: 1 wing + 1 tail, 1 wing + 1 canard, 2 wings, 1 wing no tail(flying wing). At this point in time, a traditional 1 wing and 1 tail design was chosen because it will allow for more control surfaces as compared to the other choices. As for the wing's location on the fuselage, the choices are mounting on the top, middle, or bottom. For this criteria, a high wing design would give more dynamic stability as well as more space to mount lifting rotors compared to other wing configurations. The initial configuration for the aircraft is shown in Figure 2.

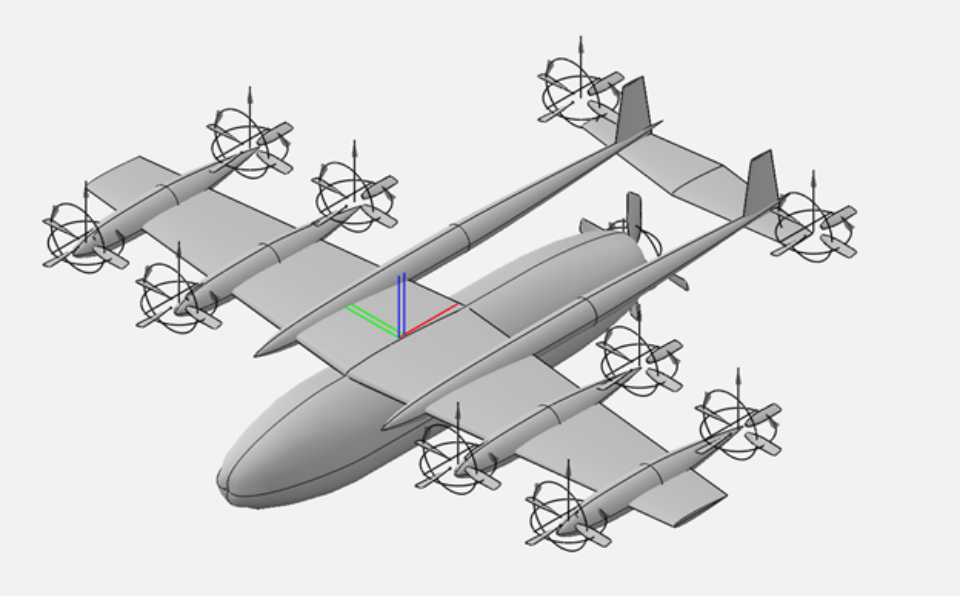

Fig. 2 Isometric View LiFT eVTOL Sketch

IV. Requirements

Table 3 Mission and Aircraft Requirements

Parameter	Value
Ceiling Altitude	2500 m
Velocity	>50 m/s
Maneuver	3 g
VTOL Thrust	25000 N
Stall Speed	<35 m/s
Range	>150 km
Climb Angle	7 Degrees
Climb Speed	6 m/s
Battery Energy Density	500 Wh/kg - Licerion[3]
Wingspan	11 m
Payload Interior Volume	3 m^3
Height	2 m
Width	1.5 m
Length	7.7 m
Number of Rotors (Lift)	10
Number of Rotors (Cruise)	1

V. Design Process

To design the vehicle, the authors employ a mixture of optimization and direct design and analyses (Figure 3).

In conceptual design, a literature survey and brainstorming are used to create conceptual ideas. Then, a weighted ranking system and direct comparisons are used to select to a single configuration. With this configuration set, the bulk of the design is calculated through the development and use of an optimization program. However, due to time constraints, not all of the disciplines are integrated into the optimization. Using the results of the optimization, the authors perform individual design and analyses for the wing twist distribution and airfoil selection, propulsion, structures, and cost. The optimization program and these additional models are detailed in the following sections.

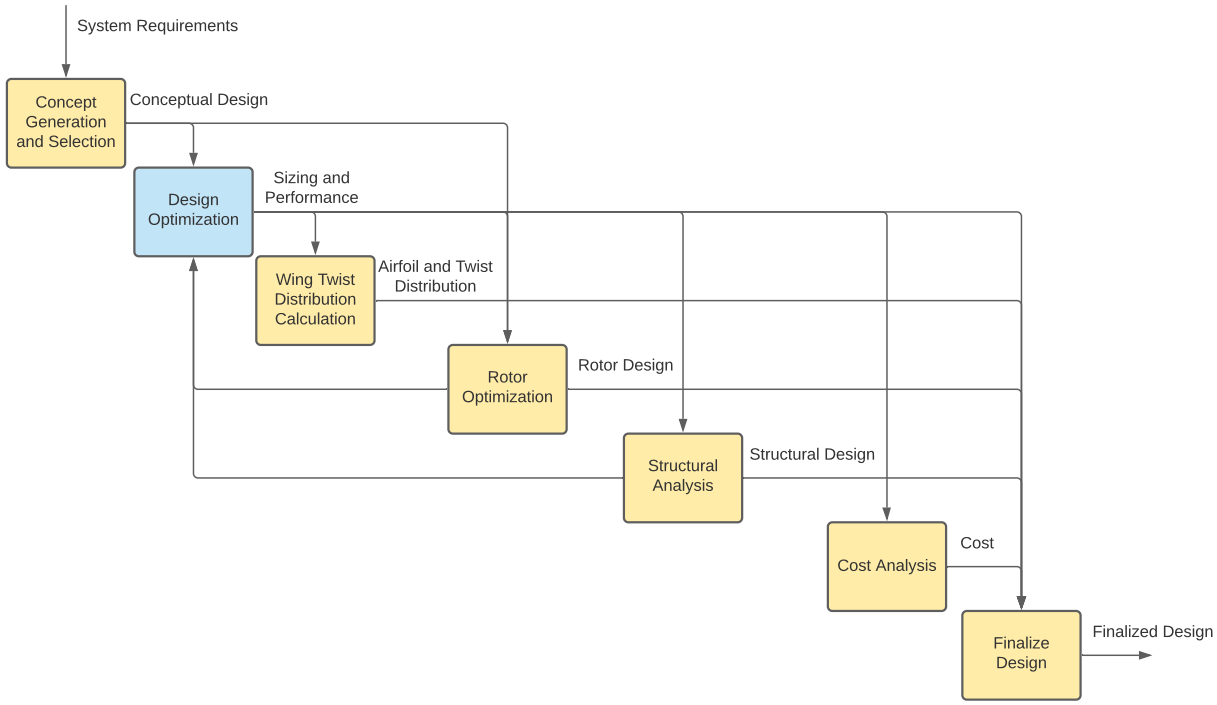

Fig. 3 Flowchart for the design process

VI. Optimization

A. Optimization Formulation

To develop the design, a low-fidelity optimization program is developed using OpenMDAO [4] (Figure 4). On top of OpenMDAO, OM Tools is used for the individual components for accurate and efficient optimization using automatically calculated analytic derivatives.

The optimization problem seeks to maximize range. The design variables include variables for sizing, wing, horizontal and vertical stabilizers, fuselage, and tail boom. Additionally, the locations of each of these components, are included as design variables. It should be noted that the sizing of the fuselage and tail boom affect the design space of the locations of the components. Lastly, this optimization accounts for operating constraints, feasibility constraints, and stability constraints (Table 4).

By developing a low-fidelity model that could run in the order of 10s seconds on a personal laptop. The authors find run-time to be particularly important as it allows the user to easily and frequently test different design configurations.

Table 4 Optimization Formulation

Objective	Range*-1
Design variable	Wingspan
Design variable	Wing mean aerodynamic chord (MAC)
Design variable	Horizontal stabilizer span
Design variable	Horizontal stabilizer MAC
Design variable	Vertical stabilizer span
Design variable	Vertical stabilizer MAC
Design variable	Fuselage length
Design variable	Tail boom length
Design variable	Cruise battery weight
Design variable	Wing center of gravity (CG)
Design variable	Vertical stabilizer CG
Design variable	Battery CG
Constraint	0.1 m <= Wingspan <= 11 m
Constraint	0.1 m <= Wing MAC <= 10 m
Constraint	2.5 m <= Horizontal stabilizer span <= 8 m
Constraint	0.05 m <= Horizontal stabilizer MAC <= 4 m
Constraint	2.5 <= Horizontal stabilizer aspect ratio (AR) <= 5
Constraint	0.05 m <= Vertical stabilizer span <= 6 m
Constraint	0.05 m <= Vertical stabilizer MAC <= 3 m
Constraint	2.5 <= Vertical stabilizer aspect ratio (AR) <= 3
Constraint	4 m <= Fuselage length <= 10 m
Constraint	0.001 m <= Tail boom length <= 6 m
Constraint	Stall speed <= 35 m/s
Constraint	CL <= 1.25
Constraint	0 N < Cruise Battery weight <= 7260 N
Constraint	0.3 <= Wing CG (Normalized by fuselage length) <= 0.6
Constraint	0.5 <= Vertical stabilizer CG (Normalized by tail boom length) <= 0.9
Constraint	0.08 <= Battery CG (Normalized by fuselage length) <= 0.9
Constraint	1.5 m <= Distance between horizontal stabilizer and fuselage
Constraint	Stability Constraints (See tables 8 and 9)
Assumed optimum	Wing taper ratio = 0.45
Assumed optimum	Wing sweep angle = 0 deg

The optimization is implemented with a series of low-fidelity models that use high-level aircraft parameters. These models were chosen to be used initially due to their fast evaluation times and ease of implementation.

B. Optimization Loop

In each optimization loop, the design variables and inputs are used to calculate key parameters such as aspect ratios and wetted areas. These parameters, along with the cruise velocity, are then fed into a weight model and a parasite drag model. Additionally, the aircraft parameters are fed into a model that estimates the Oswald Efficiency Factor. The outputs of each these models are used to explicitly calculate the optimal aircraft lift coefficient and cruise velocity. Next,

the static and dynamic stability coefficients are calculated. Following this, an additional component is included to calculate key parameters such as the stall speed and lift-to-drag ratio. Finally, these parameters are used to calculate the range, which serves as the optimization objective. An OpenMDAO-based fixed point iteration solver, the Nonlinear Block Gauss Solver, is applied to each coupling group. Specifically this solver is used to resolve the coupling from the feedback of the cruise velocity to weight model, and a nested solver is used to resolve the coupling from the feedback of the cruise velocity into the parasite drag model. Lastly, this solver is also used to resolve the coupling within the weight model due to the gross weight being an input into the weight model. An N2 diagram for the optimization is shown in Figure 4, and more detailed description of each model is described in the following subsections.

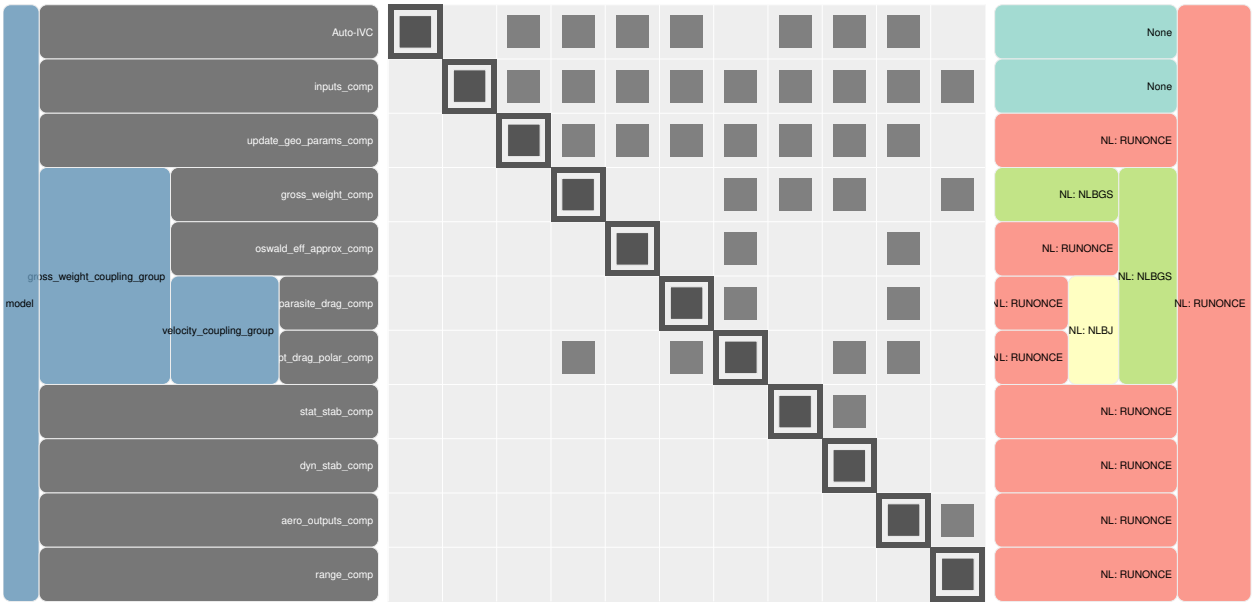

Fig. 4 N2 diagram for the optimization program

C. Weights

One part of the optimization script is the weight model for the individual components of the aircraft. A good estimate of the gross weight of an aircraft is essential to preliminary design, since the weights and stability greatly affect the performance of the design. Some of component weights in the aircraft were estimated using the mission requirements and available technology, like the payload or battery weights. Others, like the motor weights, come from analytical weights from a survey of motors with similar specifications to what the propulsion system requires. As for the weights of components that have not yet been sized, like the lifting surfaces and the fuselage, the weight model uses an empirical approach.

In order to obtain estimates of weights for components like the wing, the tail, or the fuselage, looking at past designs was very useful. Many empirical formulas for all these component weights exist and are found by a combination of analytical and statistical methods by examining old aircraft of a similar configuration and mission. Below is one such equation from Raymer's *Aircraft Design* [5].

$$W_{wing} = 0.036 S_w^{0.758} W_{fw}^{0.0035} \left(\frac{A}{cos^2\Lambda}\right)^{0.6} q^{0.006} \lambda^{0.04} \left(\frac{100t/c}{cos\Lambda}\right)^{-0.3} (N_z W_{dg})^{0.49}$$

The formula above takes into account the geometric properties of the wing, the wing's battery weight, the nominal flight condition, and the maximum loading. The gross weight of the aircraft is also implicit in the formulas for the weights of the lifting surfaces and the fuselage, so a fixed point iteration was used to generate the weight distribution for a single iteration of the optimization script. The final values generated by the optimization script can be seen in Table 5.

Table 5 Weight distribution for main components of LiFT aircraft

Gross Weight	**2100.0 kg**	**Fraction**	**Derivation**
Battery Weight	800.0 kg	38.1%	Range Equation
Payload Weight	500.0 kg	23.8%	Design Reqs.
Wing Weight	151.1 kg	7.2%	15.46[5]
Horizontal Tail Weight	6.0 kg	0.3%	15.47[5]
Vertical Tail Weight	2.3 kg	0.1%	15.48 [5]
Fuselage Weight	206.5 kg	9.8%	15.49 [5]
Tail Boom Weight	13.0 kg	0.6%	Carbon Fiber Density
Motor Weight	321.0 kg	15.3%	Part Sourcing
Miscellaneous Weight	99.9 kg	4.8%	

After finding the weights of the individual components, the locations of each were varied within the aircraft to achieve static and dynamic stability, which will be discussed in the next section. The optimization also places a constraint on the tail volume coefficients to ensure the relative sizing and location of the wing and tail are within reason (Table 13). The final component locations and weight distribution are shown in Table 6.

Table 6 Location of aircraft components and their centers of gravity

Component	Weight [kg]	CG (from nose) [m]	CG (% fuselage)	Composition
Wing	751.1	3.23	44.7%	Wing + battery*0.5 + 8 motors
Horizontal Tail	56.0	9.23	127.8%	Horizontal Tail + 2 motors
Vertical Tail	2.3	8.23	114.0%	Vertical Tail
Fuselage	706.5	3.61	50.0%	Fuselage + Payload
Cruise Propeller	71.0	7.47	103.5%	1 cruise motor
Tail boom	13.0	6.23	86.3%	Tail boom
Battery + Misc.	499.9	0.58	8.0%	Battery*0.5 + Misc. weight

D. Static and Dynamic Stability

Many constraints have to be met in order to achieve both static and dynamic stability. One of the first constraints one can check to ensure static stability is the static margin, where a value between 10% and 20% indicates pitching moment stability. The optimization script calculates the locations of the center of gravity (CG) and neutral point (NP) of the aircraft to check the static margin constraint (Table 7). The static margin was 10.8%. A side view of the aircraft along with the CG and NP are shown in Figure 5. The figure only illustrates the longitudinal locations of CG and NP along the chord of the wing for reference as the locations since not accurately represented along the height of the aircraft.

Table 7 Center of gravity and Neutral Point

	Location (from nose) [m]	% MAC
Center of Gravity	3.06	35%
Neutral Point	3.19	46%

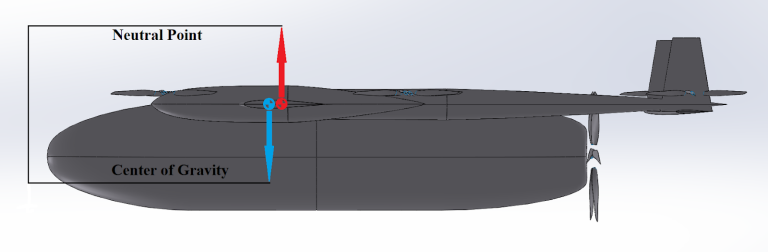

Fig. 5 Side view of LiFT aircraft with center of gravity and neutral point

After estimation of the weight distribution and component locations, another criteria to examine is the static stability of the aircraft. Equations from Dr. Anderson's MAE 155A lectures were used to calculate the stability derivatives and the results are shown in Table 8. The table also shows the constraints used in the optimization script. Many of these constraints are greatly affected by the relative sizing and locations of the wing and tail surfaces. The final outputs for these derivatives meet the criteria for static longitudinal and lateral-directional stability. In the future, simulations of the aircraft will give more refined estimates of the stability derivatives.

Table 8 Static stability derivatives for longitudinal and lateral-directional stability

Type		Value	Constraint
Longitudinal	$C_{m\alpha}$	-0.58	(<0)
	$C_{L\alpha}$	5.36	(>0)
	C_{mq}	-19.9	(<0)
Lateral	C_{lp}	-0.72	(<0)
	$C_{l\beta}$	-0.02	(<0)
Directional	$C_{n\beta}$	0.62	(>0)
	$C_{y\beta}$	-0.11	(<0)
	C_{nr}	-7.87	(<0)

The next step was to estimate dynamic stability criteria. We calculated the dimensional stability derivatives needed for estimating dynamic stability using Dr. Anderson's MAE 155A lecture notes. Mass moments of inertia for the aircraft were estimated using Raymer [5]. Dynamic stability characteristics for the short-period, Dutch roll, roll subsidence modes are shown in Table 9. The table also shows the constraints used in the optimization script for each of the dynamic characteristics. The characteristics each mode meet the criteria for dynamic stability. Two modes that were not considered were the longitudinal phugoid mode and the lateral spiral mode. Since these two modes have much longer periods, our team elected not to analyze them because the aircraft is meant to be autonomous, and so software could easily handle stability for these modes if needed.

Table 9 Dynamic stability characteristics for LiFT aircraft

Mode	Dynamic Characteristic	Value	Constraint
Short-period	Natural frequency	3.12 rad/s	$2.0 < \omega_n < 4.0$ rad/s
	Damping	0.51	$0.4 < \zeta < 1.0$
Dutch roll	Natural frequency	3.02 rad/s	$\omega_n > 1.0$ rad/s
	Damping	0.2	$\zeta >= 0.2$
Roll subsidence	Time constant	0.16 s	$\tau < 2.0$ s

E. Oswald Efficiency Factor Model

The Oswald Efficiency factor model is based on an approximation method developed by Scholz at Hamburg University [6]. The model uses an empirical formula based on prior data, and adds additional correction factors to account for the effects of the fuselage, parasite drag, and mach number. In this model implementation, the correction factors were chosen based on suggested values for general aviation aircraft (Table 10).

Table 10 Oswald Efficiency Factor Correction Factors

$K_{e,F}$	0.971
$K_{e,Cd0}$	0.804
$K_{e,M}$	1

F. Parasite Drag Model

The parasite drag model is the drag build-up model, as described by Raymer [5]. The model calculates a skin friction coefficient for each component. There is currently a limitation in using OM Tools to implement if statements within code, so skin friction coefficient calculation assumes that 20 percent of the flow is laminar and the other 80 percent is turbulent. Each of these components is normalized by the ratio between the wetted area of the component and the reference area, and multiplied by a form factor. These components are then summed together, and multiplied by an interference factor. In addition, to account for the drag from the VTOL rotors, a constant drag coefficient of 0.1 is added. This value is a rough estimation based on the results from Dundar's [7] design results.

G. Ideal Lift Coefficient and Cruise Velocity Calculation

The ideal lift coefficient and cruise velocity are calculated analytically using the resulting equations from taking the derivative of the lift-coefficient-to-drag-coefficient ratio and setting it equal to zero. By doing so, the lift-to-drag ratio is maximized, which is assumed to provide the greatest range for the electric aircraft.

H. Range Model

The range is calculated using the Breguet range equation as adapted to electric aircraft:

$$Range = \frac{\eta}{g}\frac{E}{m_b}\frac{L}{D}\frac{W_b}{W_0}$$

In this equation, η is the propulsive efficiency, g is the gravitational constant, $\frac{E}{m_b}$ is the battery energy density, $\frac{L}{D}$ is the lift-to-drag ratio, and $\frac{W_b}{W_0}$ is the battery weight ratio. An explicit calculation is viable because the range is the optimization objective, and all of the other variables are either inputs or calculated states of the optimization. Finally, the range is reported as 80 percent of the calculated range to account for preserving battery life.

VII. Additional Design and Analyses

A. Wing Twist and Airfoil Distribution

Using the outputs for the wing sizing, gross weight, and flight condition from the optimization script, an optimal span-wise C_l distribution can be calculated by approximating it to an elliptical lift distribution (Figure 6). The authors' initial idea was to vary the airfoil shape along the span in such a to maximize the lift/drag ratio given the C_l for that particular span-wise location. Upon visual inspection of the distribution, C_l did not change as much as expected, so instead of generating an airfoil distribution, the authors decided to vary the twist instead. The selected airfoil was a NACA 4412 (Figures 7 and 8), which aligned well with the average C_l span-wise value for our flight condition. Figure 9 represents a twist distribution for the NACA 4412 which would correspond to the individual points in the C_l distribution. From the figure, the wing would have to be mounted at 5 deg to the fuselage in order for the aircraft to trim with the fuselage at zero angle of attack.

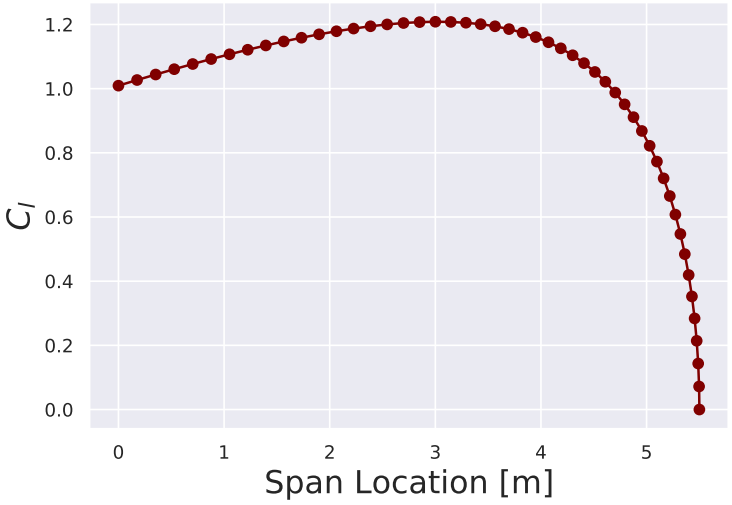

Fig. 6 C_l distribution vs. span location

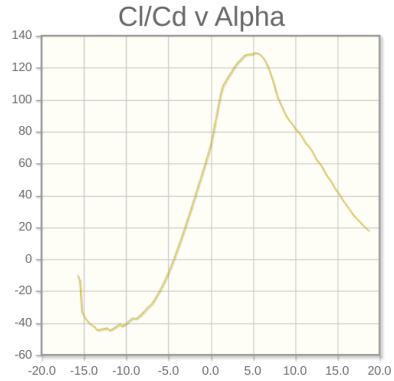

Fig. 7 NACA 4412 C_l vs. α

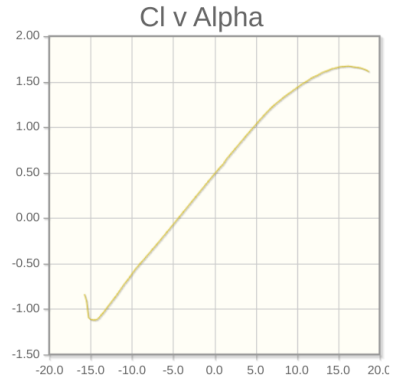

Fig. 8 NACA 4412 C_l/C_d vs. α

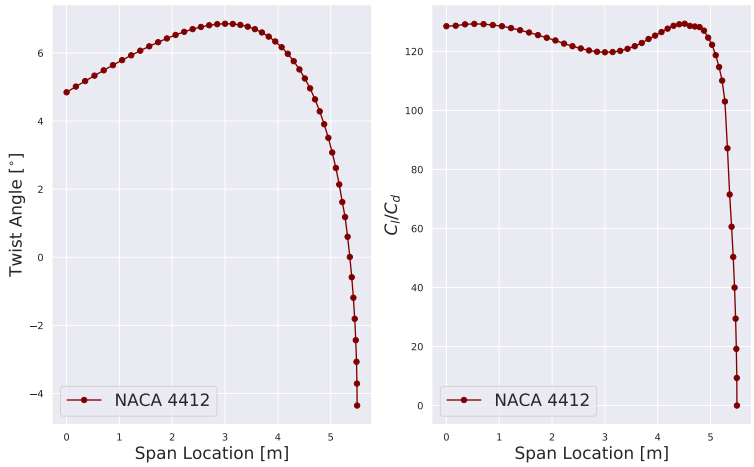

Fig. 9 Twist and C_l/C_d distribution vs. span location for NACA 4412

Figure 9 also includes C_l/C_d ratio as a function of span location. The L/D ratio ratio drops significantly for the NACA 4412 near the tip of the wing because the cambered airfoil is less efficient for the low C_l given near the tip. For that reason, the last 0.5 m of the span was switched to a symmetric airfoil, NACA 0012 (Figures 10 and 11). The new twist and L/D distribution is shown in Figure 12. As for the discontinuity in the twist distribution, the airfoils would need to be blended together in the future to ensure there are no large changes in the airfoil shape along the span.

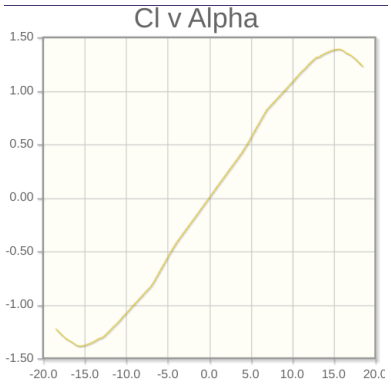

Fig. 10 NACA 0012 C_l vs. α

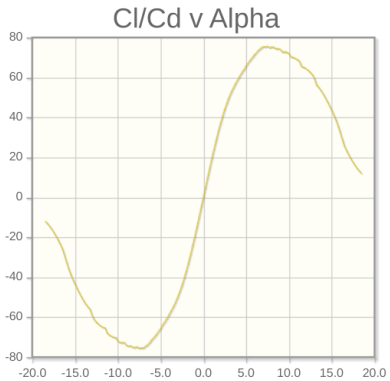

Fig. 11 NACA 0012 C_l/C_d vs. α

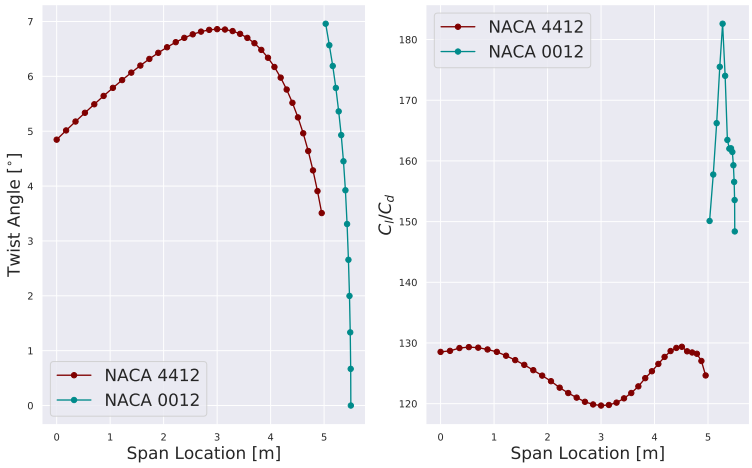

Fig. 12 Twist and C_l/C_d distribution vs. span location for NACA 4412 and NACA 0012

B. Propulsion and Rotor Optimization

During the preliminary design review, the goal was to find the minimum power the cruise and VTOL motors required to meet required flight conditions. However, for the critical design review, the goals expanded to also ensure safety with redundant systems. Both the VTOL and cruise rotors were designed using the lsdo_rotor optimizer to optimize torque and twist and chord distributions for a given propeller configuration.

1. Vertical Propellers

The power required for the VTOL motors was first found by finding the thrust required from each of the 10 VTOL motors. We used a thrust-to-weight ratio of 1.25 to ensure the motors can produce enough thrust to accelerate to the mission required 6 m/s vertical take off. This also ensures that the VTOL motors will allow for a safe descent if one were to fail during a mission. The lsdo_rotor optimization script takes in required thrust, number of propellers, propeller radius, and airfoil shape to produce minimal torque by changing the blade shape. Running multiple iterations of the lsdo_rotor optimizer, the VTOL motors were chosen to have 4 propeller blades with a diameter of 2 meters rotating at 2000 rpm. The optimization was done at rest, leading to an efficiency of 0. The twist angle and chord distribution as a function of the radius of the propeller can be seen in Figure 13. Additionally, the Reynolds number, efficiency, thrust coefficient, and power coefficient are shown as functions of the blade radius in Figure 14. Each of the propulsion parameters were calculated under the assumption of standard atmospheric conditions.

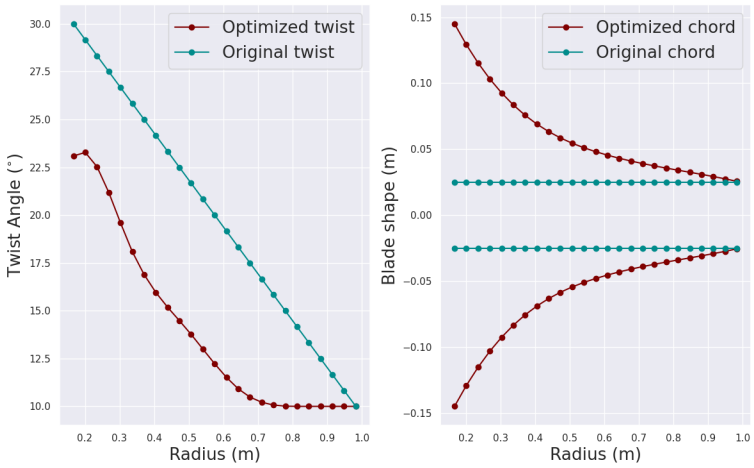

Fig. 13 Optimized twist angle and blade shape vs. rotor length for VTOL motors

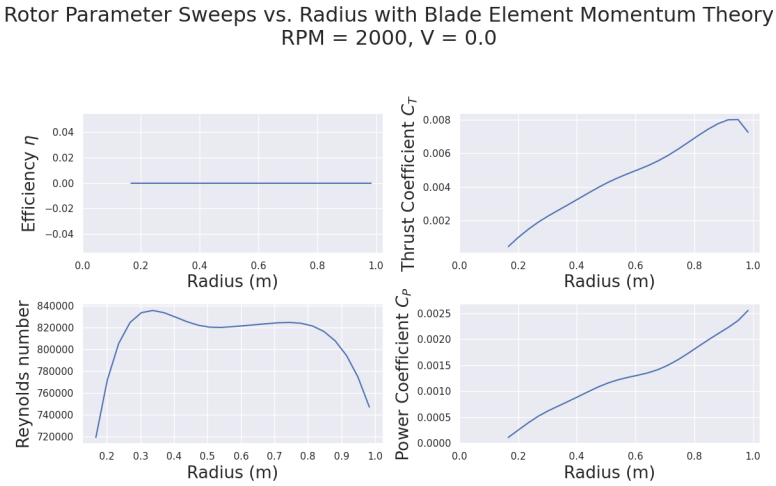

Fig. 14 Optimized efficiency, thrust coefficient, Reynolds number, and power coefficient vs. rotor length for VTOL motors

Looking at Table 11, the power required by each rotor is 45.5 kW meaning that the total required power at our set thrust is 455 kW. There is currently not a commercially available motor that will meet the requirements, so one will need to be designed and produced in order to do so. With the batteries allocated to the VTOL, this will allow for approximately 180 seconds of VTOL flight. This is 60 seconds more than the mission profile for a round trip flight, allowing appropriate room for extra VTOL propulsion if needed.

Table 11 Vertical Propulsion Parameters

Variable	Value
Number of blades	4
Propeller diameter	2 m
Rotation speed	2000 rpm
Thrust required per motor	2500 N
Torque required per motor	217.4 N-m
Power required per motor	45.5 kW
Figure of merit	0.9897
Flight time	180 s

2. Cruise Propeller

The power required was again found using steady state conditions of the vertical forces of the eVTOL to find the required thrust at steady level flight. The conditions for the steady state calculations were when the aircraft experiences its largest drag coefficient of 0.05. The motor is optimized to operate under these conditions. Using lsdo_rotor, the cruise rotor was chosen to have 4 propeller blades with a diameter of 3 meters rotating at 1800 rpm. The twist angle and blade shape as a function of the length of the propeller can be seen in Figure 15. Additionally, the Reynolds number, efficiency, thrust coefficient, and power coefficient can be seen as functions of the blade radius in Figure 16. Finally Figure 17 shows how the efficiency, thrust coefficient, and power coefficient vary with the advance ratio. All of the coefficients are again found using standard atmospheric conditions.

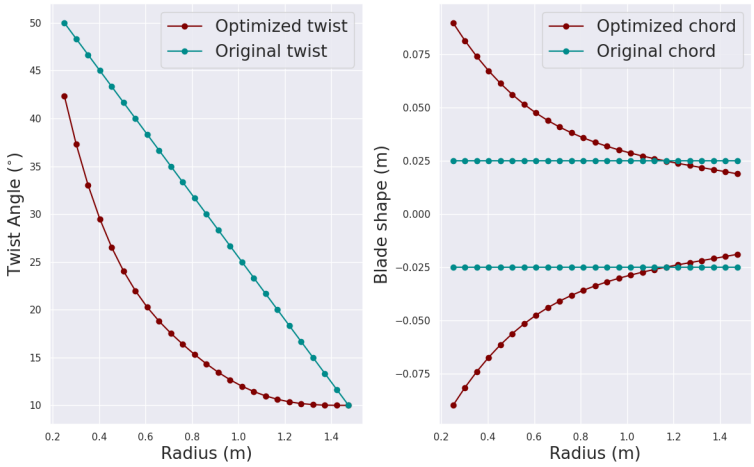

Fig. 15 Optimized twist angle and blade shape vs. rotor length for cruise motor

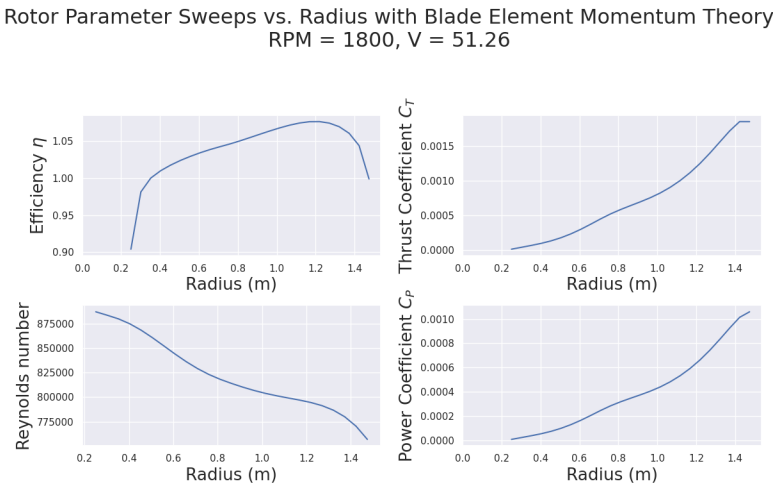

Fig. 16 Optimized efficiency, thrust coefficient, Reynolds number, and power coefficient vs. rotor length for cruise motor

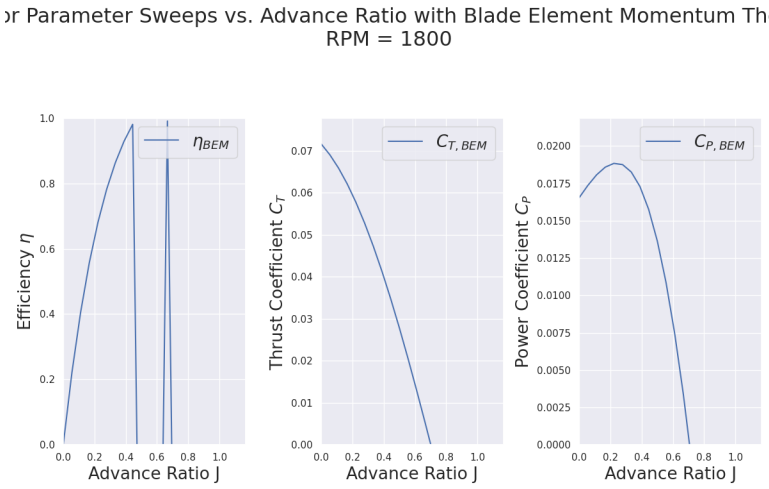

Fig. 17 Optimized efficiency, thrust coefficient, and power coefficient vs. advance ratio for cruise motor.

Looking at Table 12 the power required to operate at cruise conditions is 79.4 kW. However, the cruise motor must also be capable of operating at both climb condition and maneuvering conditions, which require more than double of the cruise condition thrust. This again is not a commercially available motor to ensure the proper requirements are met, so a motor must be designed and produced in order to do so.

Table 12 Cruise Propulsion Parameters

Variable	Value
Number of blades	4
Propeller diameter	3 m
Rotation speed	1800 rpm
Drag coefficient	0.05
Torque required	420.9 N-m
Thrust required (cruise)	1630.9 N
Power required (cruise)	79.4 kW
Thrust required (climb)	4174 N
Power/Weight (climb)	10.5 W/N
Thrust required (maneuver)	5106 N
Power/Weight (maneuver)	12.8 W/N

C. Structural Design

For this portion of the critical design review, we first decided to look at a test coupon of IM7/977-3 carbon fiber epoxy. Our first basis for designing this test coupon was by designing a rectangular plate to the dimensions of 61 cm by 15 cm, for an approximate aspect ratio of 4, we then decided to make a carbon epoxy piece that is comparable in deflection to aircraft grade aluminum. Looking at an aluminum alloy plate of the same dimensions with a thickness of .318 cm, a modulus of 68.9 GPa, Poisson ratio of .3, a yield strength of 248 MPa, and a density of 2.8 g/cm3, we can do a Navier analysis for a uniform pressure load and examine the deflection of this simply supported plate, much like it would be if it were a wing skin attached to stringers, spars, and ribs. This can be seen in the plate example below, with the Navier expansion coefficient listed next to it. This can further be used in the equation for displacement as also seen in figure 18.

$$q_{mn} = \frac{16q_0}{\pi^2 mn} \; m, n = 1, 3, 5...$$

$$W_{mn} = \frac{q_{mn}}{D[(\frac{m\pi}{a})^2(\frac{n\pi}{b})^2]^2} \quad D = \frac{Eh^3}{12(1-\nu^2)}$$

$$W_0(x, y) = W_{mn} sin(\frac{m\pi x}{a}) sin(\frac{n\pi y}{b})$$

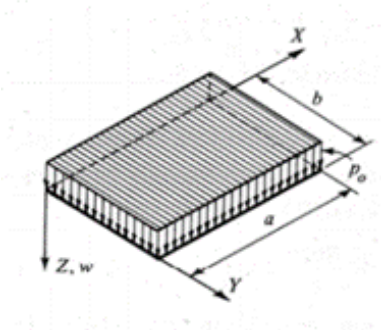

Fig. 18 Uniformly Pressure Loaded Plate with Navier Expansion Coefficient, Displacement Coefficient and Displacement Equation

Following this analysis, we can find max displacement in terms of pressure at the max point which will be the center of the plate. We find for the aluminum that the deflection is $0.0142q_0$ cm. Using the equation for stiffness (q_0A/W_0) we find that the aluminum plate has a stiffness of 2907 N/m. Knowing this stiffness for industry grade aluminum we want to see how we can match that for a carbon fiber/epoxy panel and also save weight and increase strength at the same time. This is necessary because while carbon epoxy does have a significant increase in strength over aluminum these out of plane loads still induce a lot of deflection and matching industry grade aluminum is a way for us to keep the shape of our panels in line. With this knowledge we can design a composite layup that will work for these constraints. For ease of manufacturing, we decided to only use 0, 90, and ±45 plies. After a little guess and checking we find that a 27-ply layup $[0/90/0/90/0/90/45/-45/0/90/45/-45/0/90]_s$ works well for us. IM7/977-3 carbon epoxy has properties of E_1 = 190 GPa, E_2 = 9.9 GPa, G_{12} = 7.8 GPa, poisson ratio of .35, and a density of 1.61 g/cm^3 [8]. To analyze this composite plate we need to use a different displacement coefficient as seen below.

$$W_{mn} = \frac{a^4}{\pi^4} \frac{q_{mn}}{D_{11}m^4 + 2(D_{12} + 2D_{66})(\frac{mna}{b})^2 + D_{22}(\frac{na}{b})^4}$$

Using a laminate analysis code developed in SE 142, I am able to find the D-Matrix for this laminate and plug it into the displacement code. The D-Matrix of a composite laminate is the bending stiffness matrix which is why it's components are so useful in calculating stiffness and deflection.

```
D =

   1.0e+03 *

    3.1015    0.2502    0.0297
    0.2502    2.6189    0.0297
    0.0297    0.0297    0.3779
```

Fig. 19 3x3 Bending Stiffness D-Matrix of IM7/977-3 Carbon Epoxy Laminate

Using the constraint of $.75K_{Al} < K_{carbon} < 1.25\ K_{Al}$ we find the stiffness of the carbon laminate to be 2487.4 N/m. Using strength allowable properties from the Engineering Mechanics of Composite Materials we find that this laminate has a max pressure of about 337 kPa which is equivalent to a total load over the plate of 31.4 kN. When looking at weight savings we see that the aluminum plate has a mass of 0.824 kg while the composite plate has a mass of 0.513 kg, which shows the carbon plate to be 62% the weight of the aluminum plate.

Using this knowledge, we can go on to make a V-n diagram for our aircraft. Knowing the max pressure on each of the wing panels before failure to be 337 kPa and knowing the wing area S = 22.34 m^2. Knowing this we find from a Navier analysis the load needed to cause enough deflection to cause failure in our wing skin is 2243 kN, much higher than any load this plane should be able to experience so we don't have to worry about that. Referencing the aerodynamics portion of this PDR, we know that $C_{l_{max}}$ for our Althaus AH 79-100B airfoil is equal to 1.24 and that leads to a total $C_{L_{max}}$ of 1.59 and our total mass for the aircraft to be 1323.3 kg. Using this equation from the figure below we can find a rough number for limit load to be 3.17.

Table 13.1 Typical load factors

	Category		
Load factor *n*	**Normal**	**Semi-aerobatic**	**Aerobatic**
n_1	2.1 + 24,000/(*W* + 10,000)	4.5	6.0

Fig. 20 Typical Load Factors for Different Aircraft Types [9]

Looking at the figure below we can use these equations and our parameter knowledge to develop an initial V-n diagram.

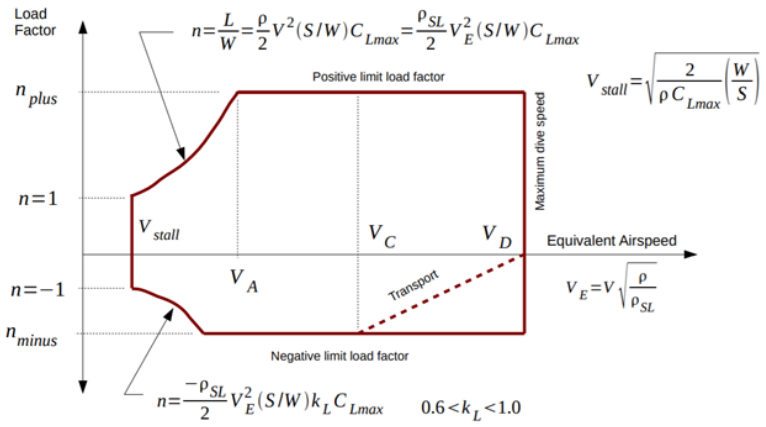

Fig. 21 Visualization of Equations Required for V-n Diagram [M. Anderson, MAE 155A Lecture 17: Air Loads, 2021]

Knowing the Mean Aerodynamic Chord of 1.16m and aspect ratio of 9.54 we can calculate the gust envelope for the said V-n diagram using these equations:

$$n = 1 \pm \left[\frac{K_g C_{L\alpha} U_e}{498 (W/S)} \right] V_e \quad K_g = \frac{0.88\mu}{5.3 + \mu} \quad \mu = \frac{2(W/S)}{\rho g \bar{c} C_{L\alpha}}$$

Fig. 22 Gust Load Factor Equations with Kg being Gust Alleviation Factor and μ being the Mass Ratio.

Using all of this, our completed V-n diagram for our aircraft can be seen below with the blue dashed line being the vertical gust load during cruise and the red dashed line being the limit of vertical gust at dive speed.

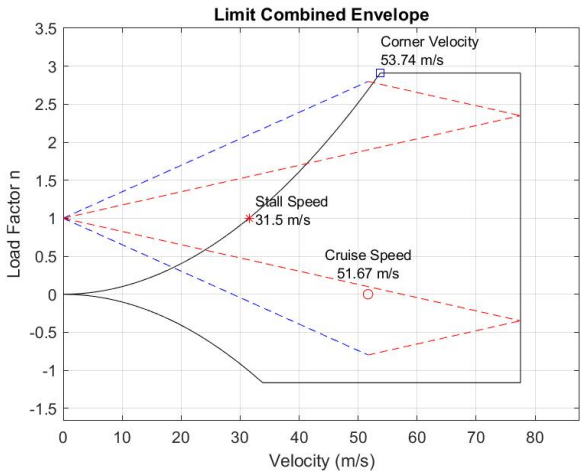

Fig. 23 LiFT eVTOL V-n Diagram

From the weights and stability section we know that the gross weight of this aircraft is to be 19645 N and from the V-n diagram the aircraft needs to withstand a loading of 2.91 g's to account for climb, corner, and dive maneuvers, this leads to a new effective weight of 57167 N. We are also incorporating a standard safety factor for passenger transport of 1.5 leading us to have to design the aircraft to withstand 85751 N of loading. Breaking it down even further, let's examine just the half span 5.5 meter long section of wing as a cantilevered beam which will be holding 36015 N or 6548.2 N/m distributed load.

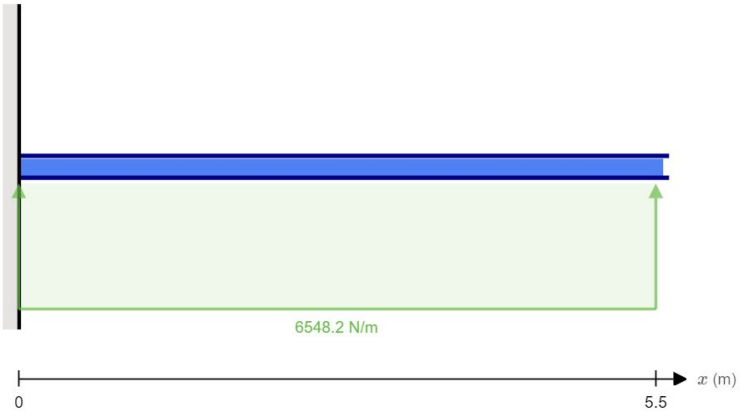

Fig. 24 Cantilevered Beam Simplification of the Wing

Looking at a design allowable for tip deflection of 5% of the half span for a deflection of .275m or 275mm [10]. We also know that the deflection equation for a beam is:

$$\delta_b = \frac{qL^4}{8EI}$$

Seeing this we can rearrange it to solve for I, the moment of inertia.

$$I = \frac{qL^4}{8E\delta_b}$$

For this build we are only using quasi-isotropic laminates meaning a balanced symmetric laminate of 0, 90, and +/- 45 degree plies leading to isotropic in plane properties[11]. Because of this we can take the modulus for IM7/977-3 to be 100 GPa. Solving for the moment of inertia using known properties and values we can find a wing moment of inertia of 2.72x10^{-}5 m^4 or 27200000 mm^4. Looking at a sample diagram of a simplified wingbox below we can see the skin is very thin (for our case 0.003429m) and does not add much and the moment of inertia equation for a rectangle to be $I = \frac{bh^3}{12}$ we find that the wing skin provides a negligible amount and for these purposes we will ignore it.

Fig. 25 Wingbox Diagram

Through this assumption we find that each spar will add an equal contribution to the moment of inertia and will be I = 1.36x10^{-}5 or I = 13600000 mm^4 for each spar. Using moment of inertia equation, we can find that an acceptable spar design can be seen in the diagram below.

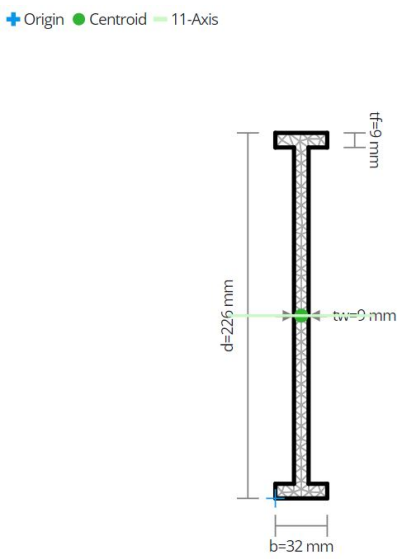

Fig. 26 Spar I beam Dimensions

Looking further we must satisfy that the web of this I beam will not buckle under loads during flight. Looking at a 26 ply quasi-isotropic sample $[0/90/0/90/45/-45/0/90/45/-45/0/90/45]_s$ and using a ritz buckling energy method with the equations for strain energy and loading below[12].

$$U = \frac{1}{2}\iint [D_{11}(\frac{\partial^2 w}{\partial x^2})^2 + 2D_{12}\frac{\partial^2 w}{\partial x^2}\frac{\partial^2 w}{\partial y^2} + D_{22}(\frac{\partial^2 w}{\partial y^2})^2 + 4(D_{16}\frac{\partial^2 w}{\partial x^2} + D_{26}\frac{\partial^2 w}{\partial y^2})\frac{\partial^2 w}{\partial x \partial y} + 4D_{66}(\frac{\partial^2 w}{\partial x \partial y})^2]\, dx\, dy$$

$$V = -\frac{1}{2}\iint N_x(\frac{\partial w}{\partial x})^2\, dy\, dx$$

$$\Pi = U + V$$

Running this analysis for total energy and finding the eigenvalues of the characteristic equation, we find that the total buckling load for this plate or spar web is $1.09\text{x}10^3$ kN which is definitely higher than what this aircraft will experience, and this sample plate is also less stiff than our actual I beam web so I see no problems with this I beam design. Looking back to the wing modeled as a beam we can see from the shear and moment diagrams below that the highest stress will be on the root or cantilevered end of the wing.

Moment Demand	$M^* = 99\,\text{kN}\cdot\text{m}$
Shear Demand	$V^* = -36\,\text{kN}$
Deflection	$\delta = 275\,\text{mm}$

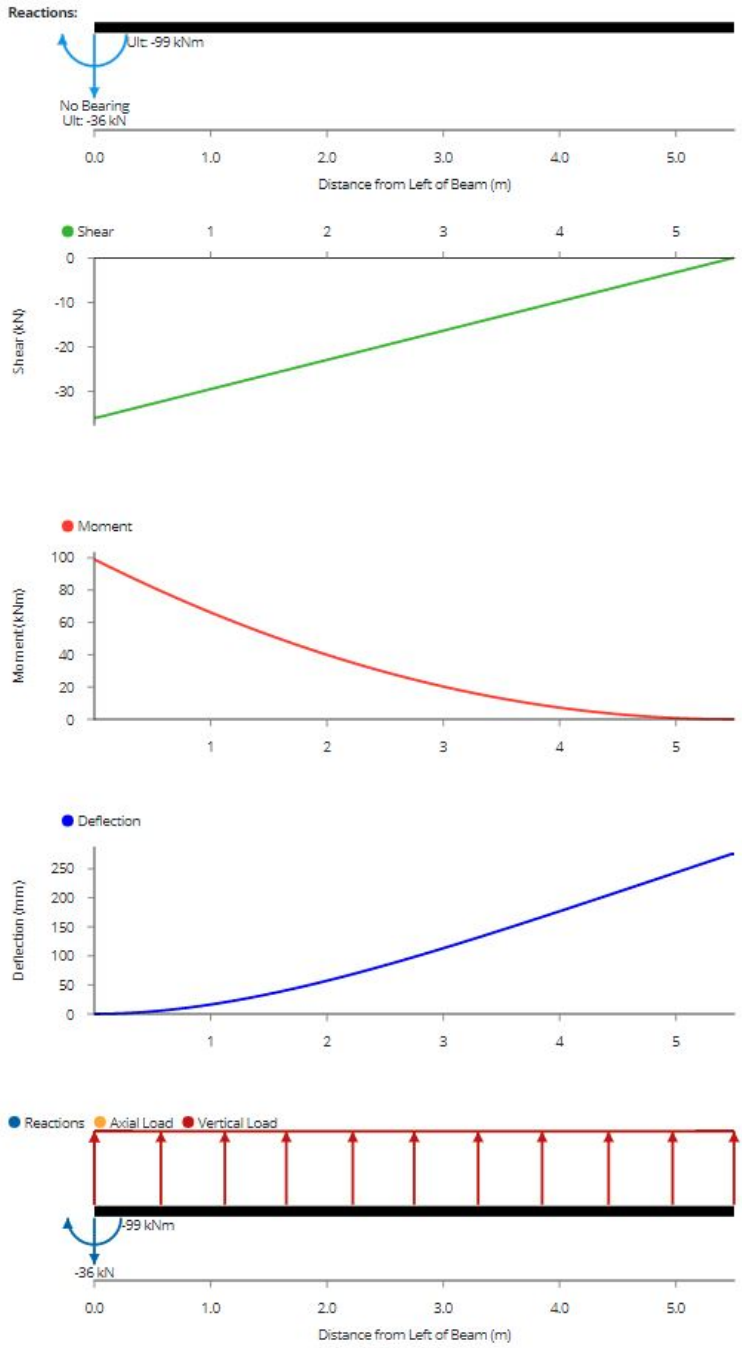

Fig. 27 Shear, Moment, and Deflection Diagrams

This is further backed up by importing a model of the wing box into ABAQUS and running a low fidelity FEA analysis on it as seen by the stress visualization below.

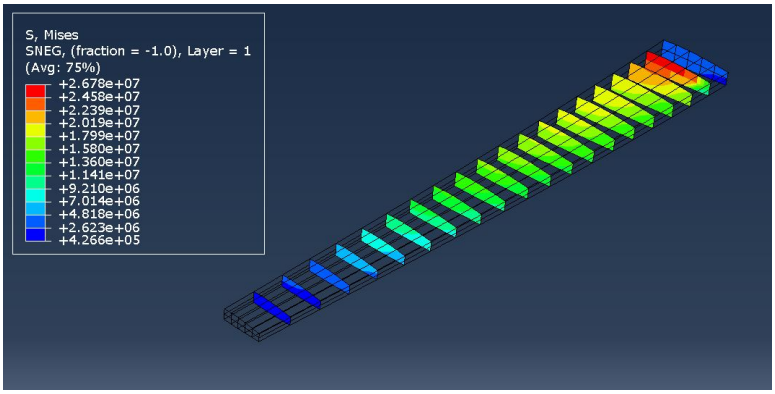

Fig. 28 ABAQUS FEA Wingbox Analysis

For our spar location we chose to do the front one at 20% of the chord and the rear one at 65% of the chord to allow for room for flaps and other control surfaces. As for spacing and design of the ribs they will be similar in thickness to the spars and be spaced out according to the wing skin analysis above 61 cm apart leading to ten evenly spaced ribs across the half span of the wing. Similarly from the wing skin analysis structural support stiffeners or stringers will be placed chord wise approximately 15 cm apart. We end up with a wing, spar, and rib configuration similar to the wireframe sketch below.

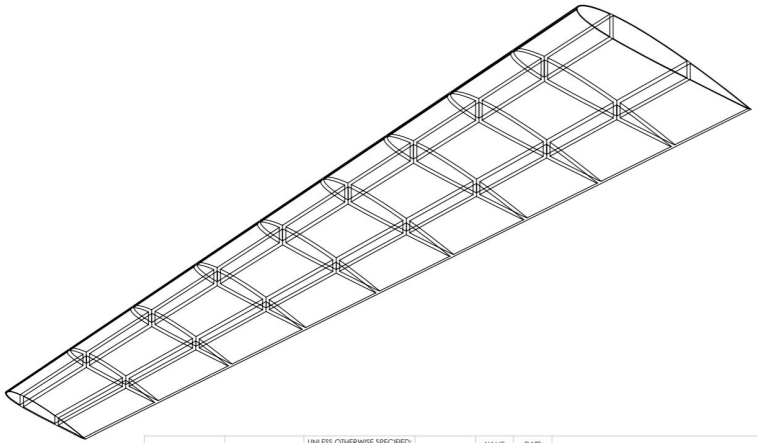

Fig. 29 Wing Drawing

We also worked up a design for the fuselage as seen in the cross sectional Figure 30 below. Our fuselage has a 2.0 m height and 1.5 m width with battery compartments underneath the floor of the cabin. It will be made of an appropriately sized carbon fiber-epoxy/Nomex sandwich panel architecture.

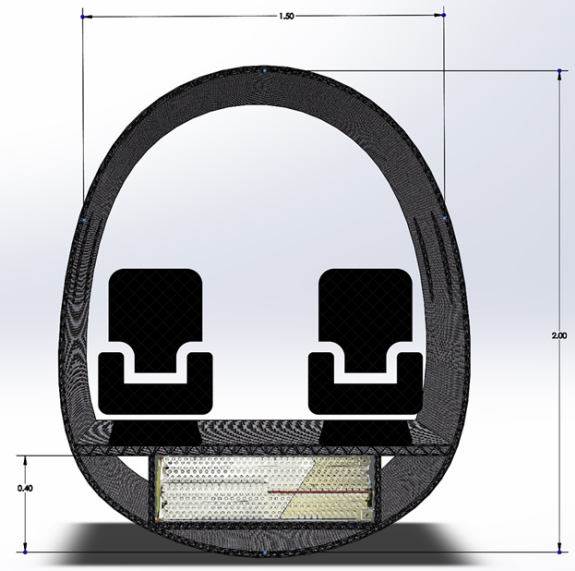

Fig. 30 Fuselage Cross Sectional View

VIII. Cost Analysis

To estimate the direct operating costs (DOC) for our LiFT eVTOL aircraft we are going to analyze pilot and maintenance technician wrap rate, material costs for maintenance, depreciation, and insurance on a per aircraft per yearly basis. For this we are estimating that each of our aircraft will fly approximately 2, 64 minute, 120 mile flights per day leading to 730 flights, 779 flight hours, and 87600 miles per year. We'll start by looking at the pilot wrap rate, while this is an autonomous mission, in the unlikely possibility that something glitches or goes wrong we will have bunker pilots on standby ready to take over. Using a pilot wrap rate of $130/hr, a number of 6 aircraft per bunker pilot, and the equation below we can calculate the pilot cost on a per flight basis and convert to yearly [13] [14].

$$PilotCost = \frac{PilotWrapRateXMissionTime}{AircraftperBunkerPilot}$$

For maintenance cost we're using a maintenance man wrap rate of $60/hr at 0.7 maintenance hours per flight hour we can find the maintenance man rate for an entire year. [13] For maintenance materials we can use the following equation to calculate material cost per flight hour.

$$\frac{MaterialCost}{FlightHour} = 3.3\frac{C_a}{10^6} + 14.2 + \left[58\frac{C_e}{10^6} - 26.1\right] N_e$$

$$C_a = Aircraft\ Cost\ Less\ Engine$$

$$C_e = Engine\ Cost,\ N_e = Number\ Of\ Engines$$

For aircraft cost, we are using a model from Daniel Raymer's aircraft design textbook based on manufacturing material costs and hours.[5]

$$Aircraft\ Cost\ Less\ Engine = Mfg\ Materials\ Cost + (Mfg\ Hours * Mfg\ Wrap\ Rate)$$

$$Mfg\ Materials\ Cost = 31.2W_e^{0.921}V^{0.621}Q^{0.799}\ (2012\ Dollars)$$

$$Mfg\ Hours = 10.5W_e^{0.82}V^{0.484}Q^{0.641}$$

$$W_e = Empty\ Weight,\ V = Max\ Velocity,\ Q = Quantity\ Produced\ in\ 5\ Years$$

Next, using power figures for our aircraft and a known average electricity rate for San Diego of $0.17/kWh [15] We can calculate the dollar amount of electricity used for an aircraft over a year. We can next add on the insurance costs for

the aircraft which we have set at 2% of the total operating costs for the aircraft. Finally, we have to factor in depreciation which we are basing on a 30% value after 10 years based on the Boeing 737 family depreciation numbers.[16] The last bit of information needed is the conversion rate of 15.5% from 2012 dollars, which some of our calculations are in, to 2021 dollars for due diligence.[17]

After completing these calculations we find a pilot cost of $23.11 per flight or $16,870 per year. For manufacturing materials cost we find a cost of $1,839,185 in 2012 dollars or $2,124,259 in 2021 dollars using a quantity of 5 produced in 5 years. For manufacturing hours we find 102,109 manufacturing hours, which leads to a manufacturing cost of $5,105,469 at a $50/hr manufacturing wrap rate for a total cost of $7,229,729 per aircraft less engine. Using this and the T-motor U15L Combo KV43 engine for lift and magniX magni500 engine for cruise at $4297[18] respectively, we can use the maintenance material cost per flight hour to find $58/FH and 0.7 Maintenance hours/FH which leads to $77,900 per year. Using our propulsion analysis we find we need 534.4 kW for all the motors for 416298 kWh per year for a total yearly electricity cost of $70771. This leads to a total operating cost of $165541 per year per aircraft. At a 2% insurance rate of operating cost we find insurance to be $3311. Finally adding in 30% depreciation over ten years we multiply 0.7 by the aircraft cost divided by 10 to be $579,076 in depreciation per year. Overall, this leads to a $747,928 direct operating cost per aircraft per year. In terms of per passenger per mile we assume a full aircraft in terms of passengers for each trip and the average flights per year and we find a direct operating cost of $2.13 per passenger – mile.

IX. Results

The list of the primary results are listed in Table 13. Results for individual disciplines are presented in the corresponding sections above.

Parameter	Value	Calculation Source
Range	544230 m	Optimization result
L/D	10.96	Optimization result
Cruise velocity	50.03 m/s	Optimization result
Stall speed	35 m/s	Optimization result
Climb gradient	7 deg	System requirement
Static Margin	10.8%	Optimization result
VTOL endurance	180 s	Additional analysis
Direct operating cost	$2.13/(passenger-mile)	Additional analysis
Gross weight	20601 N	Optimization result
Fuselage length	7.22 m	Optimization result
Fuselage width	1.5 m	System requirement
Fuselage height	2 m	System requirement
Wingspan	11 m	Optimization result
Wing aspect ratio	8.86	Optimization result
Wing area	13.65 m^2	Optimization result
Wing airfoil	NACA 4412 / NACA 0012	Manual selection
Wing loading	1505.6 N/m^2	Optimization result
Wing lift coefficient	0.98	Optimization result
Horizontal stabilizer span	2.5 m	Optimization result
Horizontal stabilizer MAC	0.6 m	Optimization result
Vertical stabilizer span	1.26 m	Optimization result
Vertical stabilizer MAC	0.42 m	Optimization result

Table 13 Summary of Aircraft Parameters

X. Conclusion

The eVTOL design presented is a long-range eVTOL aircraft that can be used for a wide range of purposes. With a range of 544 km, the vehicle can be used for inter-city round trip flights. With a cruise speed of 50 m/s, the vehicle provides a speed advantage over other forms of personal or family transportation. The fuselage exceeds system requirements with an approximate payload volume of 15 m^3, providing the passengers a luxurious experience. With reasonable stability coefficients, stall speed, VTOL endurance, and a 10 VTOL rotor design, the vehicle provides strong safety in both cruise and abnormal flight conditions. Finally, the direct operating cost of the vehicle is limited to an affordable $2.13/(passenger-mile).

While this design accounts for many important disciplines, the design tools are limited in their ability to capture certain disciplines such as aeroelasticity and aeroaccoustics. Future studies can seek develop or incorporate higher fidelity models that can capture these affects. Additionally, for more optimal results, the additional analyses that are currently separate from the optimization can be incorporated into the overall optimization program.

References

[1] Arnott, R., and Small, K., "The Economics of Traffic Congestion," *American Scientist*, Vol. 82, No. 5, 1994, pp. 446–455. URL http://www.jstor.org/stable/29775281.

[2] Cantarelli, C. C., Flybjerg, B., Molin, E. J. E., and van Wee, B., "Cost overruns in Large-Scale Transportation Infrastructure Projects: Explanations and Their Theoretical Embeddedness," , 2013.

[3] Y. Mikhaylik, C. S.-K. L. L. M. L. U. S. T. K., I. Kovalev, "650 Wh/kg, 1400 Wh/L Rechargeable Batteries for New Era of Electrified Mobility," 2018. URL https://www.nasa.gov/sites/default/files/atoms/files/650_whkg_1400_whl_recharg_batt_new_era_elect_mobility_ymikhaylik_0.pdf.

[4] Gray, J. S., Hwang, J. T., Martins, J. R. R. A., Moore, K. T., and Naylor, B. A., "OpenMDAO: An open-source framework for multidisciplinary design, analysis, and optimization," *Structural and Multidisciplinary Optimization*, Vol. 59, No. 4, 2019, pp. 1075–1104. https://doi.org/10.1007/s00158-019-02211-z.

[5] Raymer, D. P., *Aircraft design: A conceptual approach*, 4th ed., AIAA education series, American Institute of Aeronautics and Astronautics, Reston, Va., 2006. URL http://www.loc.gov/catdir/toc/ecip068/2006004706.html.

[6] Njd, M., and Scholz, D., "Estimating the Oswald Factor from Basic Aircraft Geometrical Parameters," 2012.

[7] Özgür Dündar, Bilici, M., and Ünler, T., "Design and performance analyses of a fixed wing battery VTOL UAV," *Engineering Science and Technology, an International Journal*, Vol. 23, No. 5, 2020, pp. 1182–1193. https://doi.org/https://doi.org/10.1016/j.jestch.2020.02.002, URL https://www.sciencedirect.com/science/article/pii/S2215098619316489.

[8] Daniel, I., and Ishai, O., "Engineering Mechanics of Composite Materials," *Oxford Univ*, 2006.

[9] Megson, T., "Chapter 13 - Airworthiness," *Aircraft Structures for Engineering Students (Sixth Edition)*, edited by T. Megson, Butterworth-Heinemann, 2017, sixth edition ed., pp. 421–426. https://doi.org/https://doi.org/10.1016/B978-0-08-100914-7.00013-X, URL https://www.sciencedirect.com/science/article/pii/B978008100914700013X.

[10] Odeh Dababneh, A. K., "Design, analysis and optimization of thin walled semi-monocoque wing structures using different structural idealization in the preliminary design phase," *International Journal of Structural Integrity*, 2014.

[11] Plate, D., "Carbon Fiber 101: What do Isotropic, Quasi-Isotropic, and Anisotropic Mean?" *Dragon Plate*, 2019.

[12] Kim, H., "Composite Plate Buckling, Stiffness Discontinuity, and Combined Compression + Shear," *SE253B Lecture Pack 7*, 2021.

[13] Gudmundsson, S., *General Aviation Aircraft Design: Applied Methods and Procedures*, 1st ed., Butterworth-Heinemann, 2013. URL https://www.elsevier.com/books/general-aviation-aircraft-design/gudmundsson/978-0-12-397308-5.

[14] Brown, A., and Harris, W. L., "Vehicle Design and Optimization Model for Urban Air Mobility," *JOURNAL OF AIRCRAFT*, Vol. 57, 2020. URL https://www.forbes.com/sites/jeremybogaisky/2018/09/27/startup-magnix-takes-step-toward-ambitious-vision-of-commercializing-electric-flight/?sh=10bc44a714b2.

[15] "San Diego, CA Electricity Statistics," Report, Electricity Local, 2021. URL https://www.electricitylocal.com/states/california/san-diego/#:~:text=*%2D._.%2D-,Residential%20Electricity%20in%20San%20Diego,rate%20of%2015.34%C2%A2%2FkWh.

[16] Dechavanne, G., "Aircraft Values of end-of-life A320/737 families to neo/MAX," Report, Leeham News, 2014.

[17] Tool, I., "Value of 2012 US Dollars today," Report, Inflation Tool, 2021.

[18] Bogaisky, J., "MagniX Takes Step Toward Giving Small Workhorse Planes An Electric Makeover," *Forbes*, 2018.